ELSEVIER

Chemical Physics 245 (1999) 487–506

Chemical Physics

www.elsevier.nl/locate/chemphys

Polymer electro-optic devices for integrated optics

William H. Steier [a,*], Antao Chen [a], Sang-Shin Lee [a], Sean Garner [a], Hua Zhang [a], Vadim Chuyanov [a], Larry R. Dalton [b], Fang Wang [b], Albert S. Ren [b], Cheng Zhang [b], Galina Todorova [b], Aaron Harper [b], Harold R. Fetterman [c], Datong Chen [c], Anand Udupa [c], Daipayan Bhattacharya [c], Boris Tsap [c]

[a] *Department of Electrical Engineering, University of Southern California, Los Angeles, CA 90089-0483, USA*
[b] *Chemistry Department, University of Southern California, Los Angeles, CA 90089-0483, USA*
[c] *Department of Electrical Engineering, University of California, Los Angeles, Los Angeles, CA 90024, USA*

Received 31 October 1998

Abstract

Recent advances in polymer electro-optic polymers and in fabrication techniques have made possible advances in polymer optical guided wave devices which bring them much closer to system ready. The processing of a new thermal set FTC polymer and its incorporation into a high-frequency, low-V_π optical amplitude modulator are reviewed. The design and fabrication of 100 GHz modulators and their integration with rectangular metal waveguides using an anti-podal finline transition with a flexible Mylar substrate is discussed. High-speed polymer modulators with balanced outputs and the in situ trimming of the output coupler is described. More complex guided wave devices using polymers are demonstrated by the photonic rf phase shifter. Techniques for integrating both passive and active polymers into the same optical circuit without the need for mode matching is presented and demonstrated. To reduce the V_π of a polymer amplitude modulator to 1 V or under, a technique of constant-bias voltage is demonstrated. Finally, a technique to directly laser write electro-optic polymer devices is reviewed.

1. Introduction

Polymers with electro-optic (EO) properties have been under development for several years [1,2]. The interest stems from their possible large EO coefficients, their relatively low dispersion in the index of refraction in going from infrared to millimeterwave frequencies, their potential ability to integrate easily with other materials, and their potential for low cost. There are difficult chemical synthesis problems to be solved and until recently the progress has been painfully slow. However, the recent progress reported by Dalton et al. [3] has made device quality material available and driven recent progress in device applications.

EO polymers require highly optically nonlinear chromophores which can be incorporated into a polymer host, aligned by a poling electric field, and finally hardened to maintain the alignment. Highly non-linear chromophores have been synthesized and

* Corresponding author. Fax: +1-213-740-8684.

0301-0104/99/$ - see front matter
PII: S0301-0104(99)00042-7

incorporated into a polymer host but the resultant EO coefficients in devices have not been as large as expected. Dalton's recent work on the probability of large-$\mu\beta$ chromophores to aggregate into pairs and thus not contribute to an EO effect and his work on hardening the polymers after poling to prevent alignment relaxation has resulted in significantly improved materials. In this paper we will review the progress in photonic devices which rely on these improved EO polymers. Infrared high-speed modulators with V_π under 5 V and modulators operating at modulation frequencies over 100 GHz have been developed [4]. Recently we have demonstrated more complex structures than Mach-Zehnder interferometers such as rf phase shifters. Initial demonstrations have been made of integrating the EO polymer devices with high-speed silicon electronics [5] and with optical devices fabricated in other materials [6].

The dominant EO material in today's technology is clearly $LiNbO_3$. This crystalline ferroelectric material has been under development for many, many years and is now available in relatively large sizes with relatively large EO coefficients. Commercial modulators are available which operate to 10 GHz with V_π in the 5–6 V range [7,8]. Unless polymer modulators can prove to be much less expensive than the $LiNbO_3$ devices, polymers will likely not play any significant role in this type of modulator operating in this frequency range. However, the polymer materials have some significant advantages over the crystalline materials and it is the applications which rely on these advantages where the polymer devices can enter the system technology. In our view there are three advantages that the polymers have over other EO materials. In this review, we will not discuss the potential for lower-cost devices using polymer since that will largely rely on packaging and production issues and these have yet to be demonstrated.

The first advantage is the low dispersion in the index of refraction between infrared and millimeter-wave frequencies. For very wide-band, high-frequency operation the EO modulators must be traveling wave devices and therefore the issue of maintaining a velocity match between the optical wave and the mm-wave becomes important. The maximum interaction length is set when the two waves slip π out of phase. Since the dielectric properties of the polymers are all electronic in nature, $n(\text{opt}) \approx n(\text{mmwave})$, and a phase match can be maintained over a reasonable length in a simple structure. For example, at 100 GHz the polymer modulator can still be ~ 2 cm long while the $LiNbO_3$ device is limited to ~ 1 mm [4]. Successful $LiNbO_3$ modulators [9] has been demonstrated at over 70 GHz using clever velocity-matched structures to increase the interaction length. Using standard strip line and optical waveguide technology we have demonstrated a polymer modulator over 1 cm long with high overlap integral operating to 113 GHz. The close phase match comes about essentially because of the relatively low dielectric constant of polymers as compared to crystalline ferroelectrics. The low dielectric constant may make it possible to locate several individual high-speed modulators close to one another without causing degrading rf crosstalk between the modulators. This leads to the possibility of packaging several modulators in the same module for compact multi-channel optical communication links.

The second advantage of polymers as electro-optic materials is that they can be deposited onto and will adhere to many substrates including semiconductors. In addition, optical guiding structures and modulators or optical switches use fabrication techniques which are compatible with semiconductor electronics [5,10]. This makes possible a significant step forward in opto-electronic integration. A material with large EO effects and good optical quality can be integrated on the same substrate with the high-speed drive and signal processing electronics. The processing steps for the polymer devices and the temperature stability of the polymer materials are compatible with this integration. In contrast only hybrid integration using separate optical and electronic modules connected via cables or flip-chip bonding is possible using the crystalline dielectrics such as $LiNbO_3$. There are well established and highly developed VLSI semiconductor foundries from which one can have fabricated state-of-the-art high-speed integrated semiconductor electronic circuits built to your design. This technology could now become available for high-speed optoelectronic circuits by developing the techniques of fabricating the polymer optical switch/modulators and other polymer integrated optical devices onto the Si or GaAs substrate which already

contains the control, drive, and interface integrated electronics. The final steps of interconnecting the polymer optical devices with the electronics, attaching fiber inputs, and final packaging must be done using fabrication techniques compatible with the polymer and the semiconductor devices. The integration of the well-developed existing semiconductor foundry technology with the high potential of the polymer optical devices opens up a promising new approach to high-speed optoelectronics.

The third advantage is the ability to integrate the active polymer materials into an optical circuit which includes other optical materials. The key technology lies in the ability to fabricate low loss vertical waveguiding structures in the polymers [11], which can interconnect multiple layers in optical integration. Low-angle vertical shapes can be fabricated by reactive ion etching in either oxygen or CF_4. Slow vertical tapers with heights of several micrometers and lengths of a millimeter or less can be patterned and etched. This makes it possible to fabricate vertical waveguide bends and vertical waveguide power splitters which are some of the key elements to make three-dimensional integrated optics possible. More details on our work on 3D polymer integrated optics are given in a recent paper [6]. Perhaps more important in regards to EO polymer devices, these vertical structures allow one to place the active polymer material only in the region of the optical circuit where it is required. In this approach, the interconnect waveguide pattern is first fabricated in a low-loss passive polymer or other material system. The active polymer is then placed on top of this layer and patterned into the area where needed. Vertical coupling structures are then fabricated to channel the light up into the active polymer and then back down again into the passive waveguides. The adiabatic vertical couplers solve the often difficult problem of optical mode matching between the various material systems. This advantage of the polymers allows one to design complex optical circuits where the interconnects are made of materials engineered for very low optical loss and yet still include EO polymers which have been engineered for maximum EO effects.

In this paper we review some of our work on optical polymer waveguide devices which exploit the advantages outlined.

2. High-speed polymer modulators

One of the most promising of the new EO polymers developed in Dalton's laboratory uses a high-$\mu\beta$ chromophore based on a novel tricyanobutadiene acceptor incorporating a furan-derivative ring, FTC 2-dicyanomethylen-3-cyano-4-{2-[*trans*-(4-N, N-diacetoxyethyl-amino)phenylene-3,4-dibutylthien-5]-vinyl}-5,5-dimethyl-2,5-dihydrofuran) [12]. Fig. 1 shows the chemical molecular structure of the FTC chromophore. The furan ring plays an important role in keeping the conjugation planar and stabilizing the acceptor end of the chromophore. Also, the two methyl groups on the heterocyclic (oxygen) ring and the two butyl groups on the thiophene ring should prevent the large dipolar chromophores from aggregating which is caused by strong electrostatic interactions in most of the high-$\mu\beta$ chromophores. The interaction between the chromophores may reduce the achievable EO coefficients. The FTC chromophore when doped into a PMMA host has an $r_{33} \approx 55$ pm/V @ 1060 nm. The chromophore has excellent thermal stability ($> 300°C$) and the guest–host system has modest optical loss of 1 dB/cm @ 1300 nm.

To produce a device quality material with good thermal stability the FTC was incorporated into a thermal-set polyurethane system [13]. The FTC chromophore is mixed with toluene diisocyanate (TDI) in a solvent and heated to attach the NCO groups to the OH groups. Next, the crosslinker, triethanolamine (TEA), is added which acts to form a 3D network during the precuring and final hardening during poling. Excess TDI and TEA can be added to control the density of chromophores.

Alignment of the chromophores is required to achieve the EO effect and electric field poling does this. In all thermoset materials an optimum poling profile must be empirically determined. Fig. 2 shows the typical poling profile; it consists of two steps, pre-curing and poling. During the pre-curing step, the crosslinkable PU-FTC polymer is heated to temperature, T_{pre}, for the time, t_{pre}, to initiate partial crosslinking prior to applying the high voltage. This is to prevent surface damage during poling. There is a trade-off between the pre-curing time and the poling efficiency. When the precuring is not sufficient, surface damage occurs while with excessive

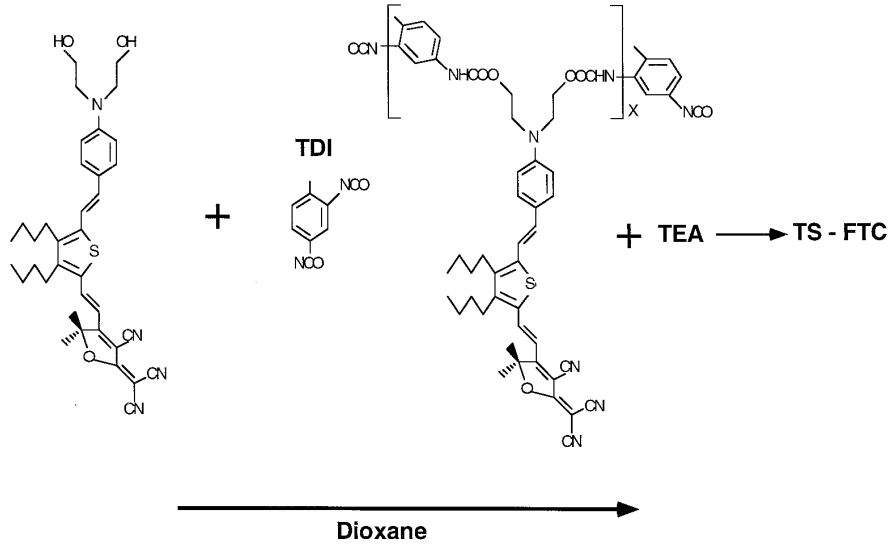

Fig. 1. The FTC chromophore and the covalent incorporation into a thermal set polyurethane polymer to form the TS-FTC. TDI and TEA are commercially available crosslinkers and dioxane is the solvent used.

pre-curing the rotation of the chromophores is restricted and the poling efficiency is reduced. During the poling step, a dc voltage, V_p is applied to the corona needle with the sample temperature fixed at T_p. Here again there is a trade-off. Higher T_p may allow easier rotation of the chromophores and allow more complete crosslinking, which gives higher poling efficiency and higher thermal stability. On the other hand, if T_p is too high the crosslinking may be achieved before the chromophores have had time to align to the electric field. The optimum poling profile is different for each thermoset polymer systems. The near optimum poling profile for the TS-FTC is $T_{pre} = 120°C$, $t_{pre} = 3$ min, $T_p = 100°C$ for 1 h with $V_p = 8$ kV. The measured r_{33} was 35 pm/V at 1060 nm. This alignment is stable to 90°C for long periods. The drop in r_{33} between the hardened polymer and the softer guest–host system is typical and is the price one pays for good thermal stability. We also measured the optical loss of the hardened TS-FTC to be ~ 2 dB/cm @ 1300 nm.

In a device, a lower cladding of passive polymer is placed between the EO polymer and the ground electrode. In the measurements discussed above the EO polymer is directly on the ground electrode. When poling multiple layers, there is always the question of whether the poling electric field is across the EO polymer or across the lower cladding. It is therefore advantageous for the cladding to have a slightly higher electrical conductivity at the poling temperature than does the EO polymer. This assures that all or most of the electric field is across the EO

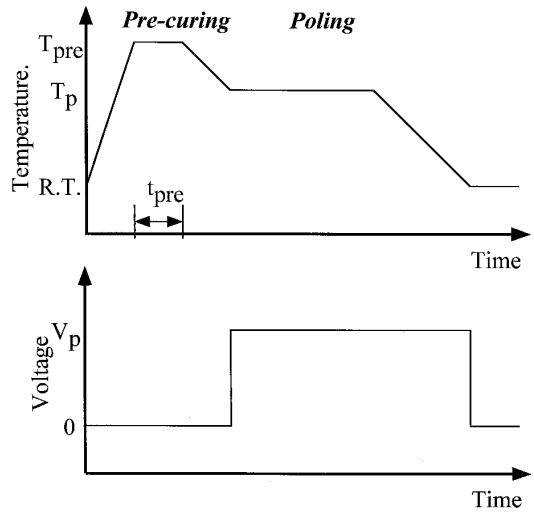

Fig. 2. Pre-curing and poling temperature and voltage profiles for TS-FTC. T_{pre} and t_{pre} are the temperature and time, respectively, used for pre-curing the material. T_p and V_p are the temperature and the corona tip voltage, respectively, used for electric field poling.

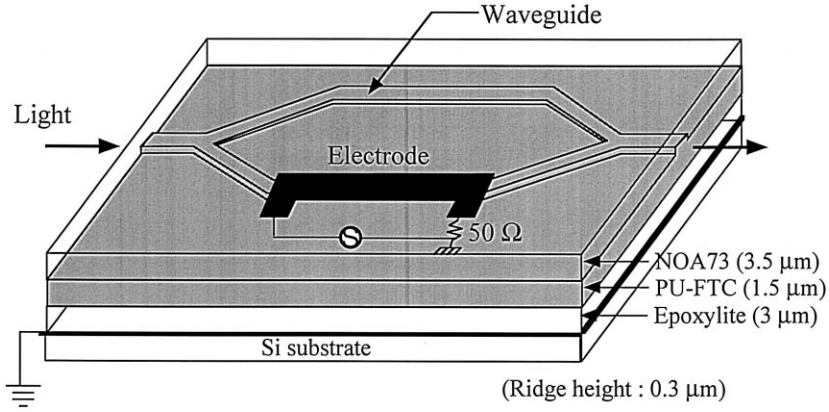

Fig. 3. Schematic of a Mach-Zehnder traveling wave optical amplitude modulator. The light is guided in the buried rib waveguides and the millimeterwave modulation signal is guided on the microstrip line.

polymer. The lower cladding must also be hardened so that it is not susceptible to the solvents used in spinning the EO polymer. One acceptable material for the lower cladding is Epoxylite 9653 [14]. We could measure no difference in the r_{33} coefficient of the EO polymer when poled directly on the ground electrode or with the intervening Epoxylite layer.

A high-speed Mach-Zehnder amplitude modulator based on the TS-FTC is shown in Fig. 3. High-speed modulators combine a traveling wave optical Mach-Zehnder interferometer and a high-speed traveling wave microstrip line circuit. For vertical confinement in the optical waveguides, a triple stack structure composed of the lower cladding, core EO polymer, and upper cladding is used. Lateral optical confinement is achieved by a rib structure etched by RIE on the core layer. Epoxylite 9653 ($n = 1.54$ @ 1300 nm) was used for the lower cladding and a UV curable epoxy, NOA73 [15] ($n = 1.54$ @ 1300 nm), was chosen for the upper cladding. NOA73 has good adhesion to the metals used for the upper electrode (Cr and Au) and it can be rapidly UV cured. The UV energy for curing is small and is highly absorbed in the NOA73 to assure no UV damage to the EO polymer occurs. In the typical device, the waveguide rib width is 6 μm, the core layer thickness is 1.5 μm, and the rib height is 0.3 μm. These dimensions provide single-mode operation at 1300 nm. The thickness of the lower and upper claddings were set at 3 and 3.5 μm, respectively, to keep the optical loss due to the electrodes small. The length of the arms of the interferometer where the modulation interaction occurs is 20 mm and the length of the linear Y-branch transition is 3 mm at each side. The total branching angle of the Y-branch is $\sim 1^\circ$ and the separation between the two straight waveguides in the interaction region is 50 μm.

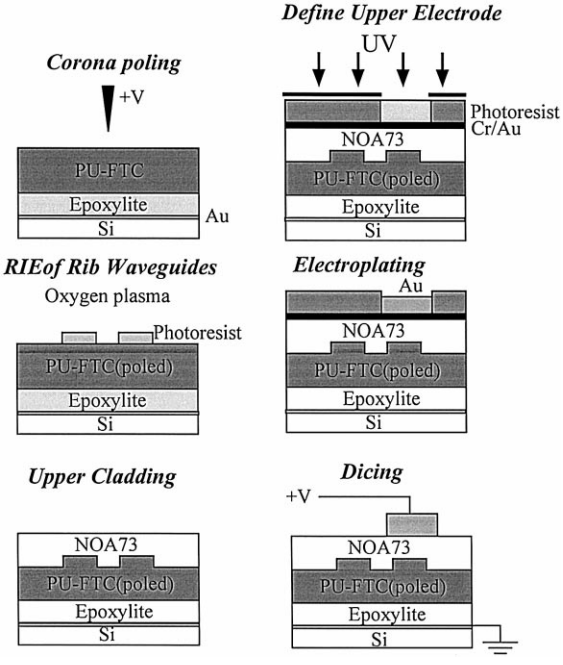

Fig. 4. Fabrication steps for the Mach-Zehnder optical modulator.

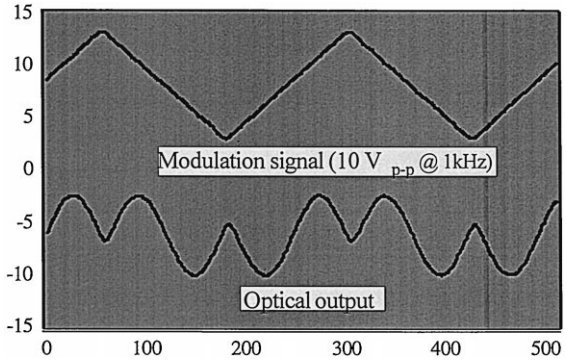

Fig. 5. Oscilloscope traces for the measurement of V_π of the FTC modulator. The upper trace is the 10 V, 1 kHz sawtooth waveform applied to the microstrip line. The lower trace is the light output from the modulator. The voltage required to go from maximum to minimum light out, V_π, can be measured. For this modulator $V_\pi = 4.5$ V.

The microstrip line is formed between the lower ground electrode and the upper electrode. Its characteristic impedance was designed to be 50 Ω by setting the width of the upper electrode to be 22 μm. To reduce the mm-wave loss, the thickness of the upper electrode was increased to ~ 4 μm by electroplating after the electrode shape was defined by lithography. A tapered pad structure, 3 mm $\times$ 150 μm, was formed at each end of the microstrip line to facilitate the attachment of the coaxial input and output cables during packaging. As the final fabrication step, the end faces were prepared for butt coupling to a fiber by dicing with a nickel blade. The fabrication steps are shown in Fig. 4.

To measure the performance of the modulator, TM-polarized light at 1310 nm was butt-coupled into the device through a single-mode fiber and the output light was collected by a microscope objective lens and focused onto a photodetector. Fig. 5 shows the response of the modulator to a low-frequency sawtooth wave electrical signal to measure, V_π, the voltage required to turn the modulator from full on to full off. The measured V_π was 4.5 V, which corresponds to an r_{33} of ~ 25 pm/V with an effective field-overlap integral factor of one. This is consistent with the r_{33} value measured at 1060 nm on test samples. Eight modulators are fabricated on a single substrate and the V_π ranged from 5.5 to 4.5 V. The extinction ratio, the ratio of the light power out during the on state to that of the off state, was measured to be 18 dB. The extinction ratio should increase when a single-mode fiber is used to collect the output rather than the lens. The measured insertion loss was ~ 14 dB for the device length of 36 mm. The total insertion loss is the sum of the waveguide propagation loss and the coupling loss at the facets. There is a ~ 5 dB/facet coupling loss since no attempt was made to match the ~ 9 μm dia. mode of the fiber to the elliptical mode (7 μm $\times$ 2 μm) of the polymer waveguide. Accordingly, the propagation loss of the waveguide is ~ 2.5 dB/cm. The waveguide propagation loss is a collection of the losses from material intrinsic absorption, waveguide/cladding layer scattering, and poling-induced scattering [16].

The variation of the modulator response from very low frequency out to 40 GHz is shown in Fig. 6. The modulator should remain velocity matched to frequencies greater than 100 GHz as we have demonstrated in our earlier work. The increased rf loss due to the upper electrode may become a factor at 60 GHz or greater. We believe the ripples in the response shown in Fig. 6 are due to impedance mismatches at the input and the output.

These modulators using the TS-FTC polymer demonstrate some of the advantages that EO polymers have long been promising. The V_π is low enough for systems interest and the frequency response is well into the millimeter wave range. One of the remaining problems is the insertion loss. The use of mode tapers and high numerical aperture fibers [17] can solve the fiber to waveguide coupling

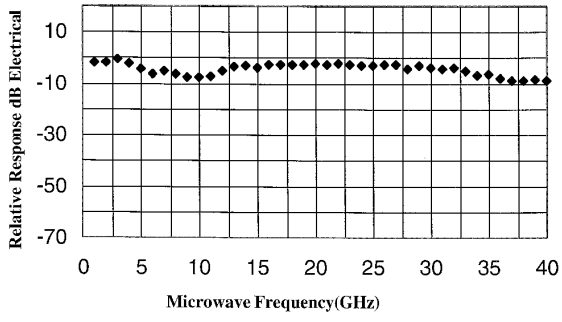

Fig. 6. The measured frequency response of the FTC Mach-Zehnder modulator.

loss. The propagation loss in the waveguides is dominated by material loss with perhaps 0.5 dB/cm due to the fabrication process. The material loss in polymers at 1300 and 1500 nm could be due to overtones of the C–H vibration band or to scattering from inhomogeneities. Previous thermal deflection spectroscopy measurements [18] in PMMA and our waveguide loss measurements in Norland polymers indicate that the loss due to the C–H vibration should be on the order of 0.3 dB/cm @ 1300 nm. We have not seen a significant difference in the loss between poled and unpoled material and therefore believe that poling-induced inhomgeneities do not play a large role. This leaves only scattering loss due to inhomogeneities during the hardening as the cause of most of the loss. Other polymer systems using other hardening schemes are now under investigation.

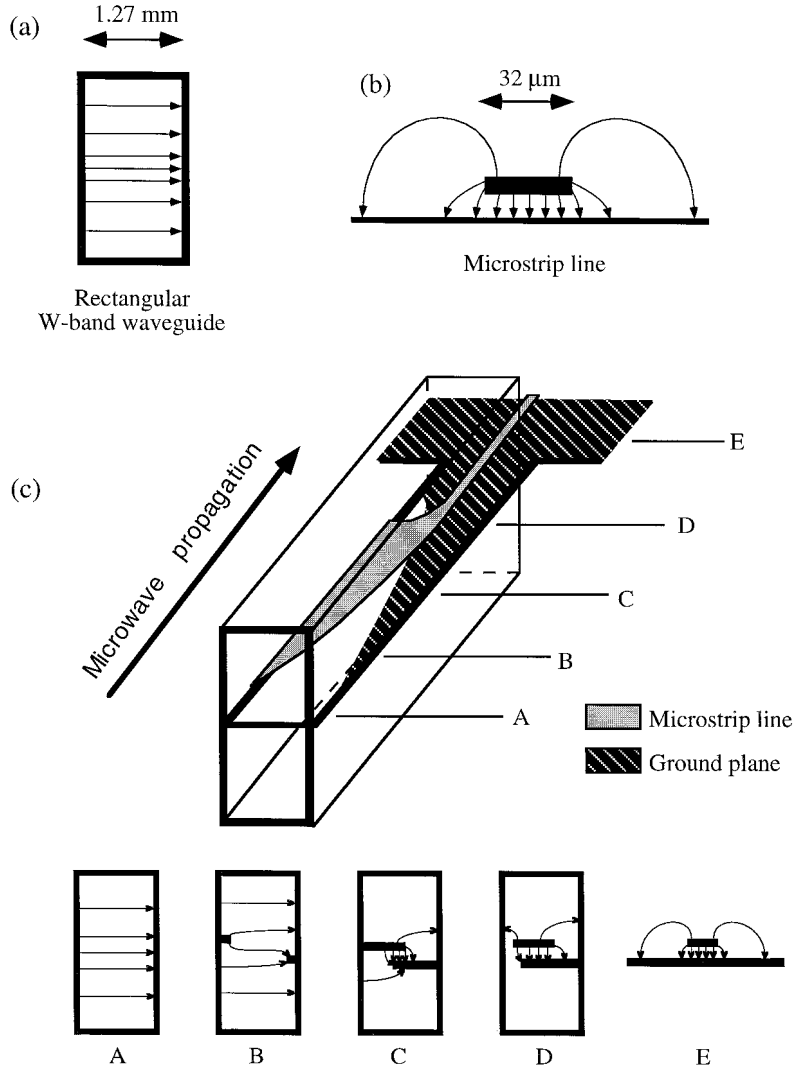

Fig. 7. The anti-podal finline transition section for converting the electric field in a rectangular metal waveguide into the required electric field for a microstrip line. Shown in (a) are the dimensions of the W band waveguide used at 100 GHz frequencies and shown in (b) are the dimensions of the microstrip line of the modulator. Shown in (c) are the cross-sections of the transition going from A, the rectangular waveguide, to E, the microstrip line.

3. Advanced high-speed modulator designs – Modulators on flexible substrates

At modulation frequencies greater than ~ 70 GHz, the packaging of polymer high-speed modulators requires novel approaches. Millimeter wave transmission lines from sources or from antennas at these frequencies are typically rectangular hollow metal waveguides whose cross-sectional dimensions are on the order of a few millimeters. In contrast, the millimeter wave transmission line in the polymer modulator is a microstrip line. To couple between the two very different types of transmission lines requires novel broadband structures. We recently designed and demonstrated [19] an integrated anti-podal finline transition structure as shown in Fig. 7. It has the advantage of low-loss and high-dimensional fabrication tolerance. The transition gradually transforms the electric field profile of the rectangular metallic waveguide to that of the microstrip line electrode on the device and effectively couples the microwave driving power into the modulator. This structure must be inserted into the small W-band rectangular waveguide (1.25 mm × 2.5 mm) and therefore the thickness of the substrate must be kept as low as possible. For lower-frequency modulators the substrate thickness is not an issue since coaxial rf connectors are used and we therefore typically fabricate the modulators on relatively thick silicon substrates. For the high-frequency modulator using the anti-podal finline coupler, the substrate must be a thin dielectric with low microwave loss as well as good electrical, chemical, thermal and mechanical properties. Among a wide range of substrates considered, a 127 μm thick Mylar film closely matched our conditions. The film was mounted on a silicon substrate for mechanical support during processing. The gold ground plane was deposited on the Mylar and using standard photolithography techniques, the lower finline transition pattern was then etched in the region to be inserted into the waveguide. The lower cladding layer and the active polymer layer were spin coated on the substrate and the active polymer was corona poled. The optical waveguide pattern was defined on the polymer using reactive ion etching with alignment to the pre-etched ground pattern. The upper cladding was then spun on and a thin layer of chromium and gold was deposited for the top electrode. A thick photoresist was patterned to define the top electrode and the upper finline transition region. This pattern was precisely aligned to both the polymer optical waveguide and the lower finline. Electrochemical gold plating was used to increase the thickness of the top electrode to 7 μm. Fig. 8 shows the array of modulators. The particular finline transition region to be inserted into the rectangular waveguide was separated from the array and the polymer layers on the lower finline transition pattern removed using a solvent that was locally applied. The transition was then inserted into the waveguide. A photograph of the packaged device is shown in Fig. 9.

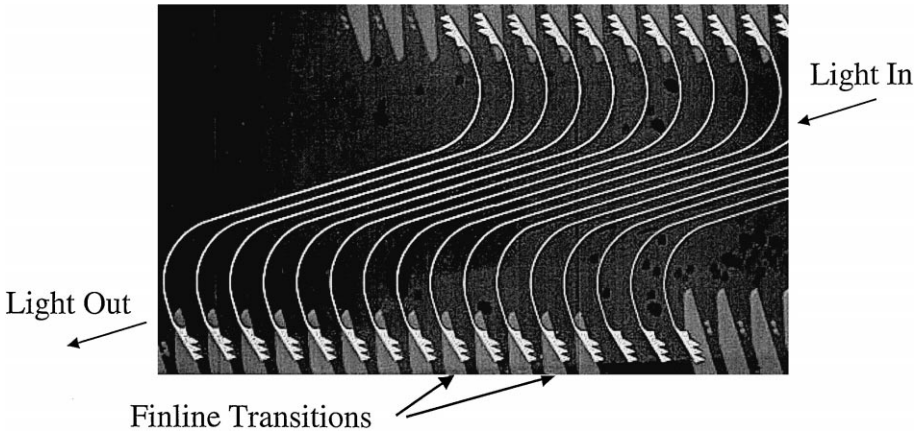

Fig. 8. Photograph of an array of polymer phase modulators built on the Mylar substrate with the anti-podal transition sections on each end. The buried rib optical waveguides cannot be seen in the photograph.

In this modulator we used an amino phenylene isophorone isoxazolone (APII) chromophore developed in Dalton's laboratory [20]. The chromophores are incorporated into a crosslinked polyurethane thermosetting network similar to that used with the FTC chromophore. The optimum loading density of the APII chromophore in polyurethane thermoset is 40 wt%, which is much larger than corresponding values for other high-$\mu\beta$ chromophores. The polymer has an EO coefficient of $r_{33} = 30$ pm/V and an optical loss of ~ 1 dB/cm at an optical wavelength of 1060 nm.

The performance of these integrated finline coupled modulators was measured using an optical heterodyne technique [21]. This technique involves mixing of the modulated output of our device and the output of a tunable laser that is set at a fixed frequency away from the center frequency of the modulated laser beam. This effectively down converts the millimeterwave modulation frequency by the difference frequency between the two lasers. The frequency measured by the detector is therefore much lower and thus alleviates the need for a detector which can respond to millimeterwave frequencies. Fig. 10 is the spectrum analyzer trace of the down converted signal at 95 GHz. These modulators were configured as birefringence modulators and had a V_π of 16 V. Since birefringence modulators rely on the difference in the EO coefficients $(r_{33} - r_{13})$, if we assume the usual condition that $r_{33} = 3r_{13}$ this material should have a V_π of ~ 10 V in a Mach-Zehnder configuration.

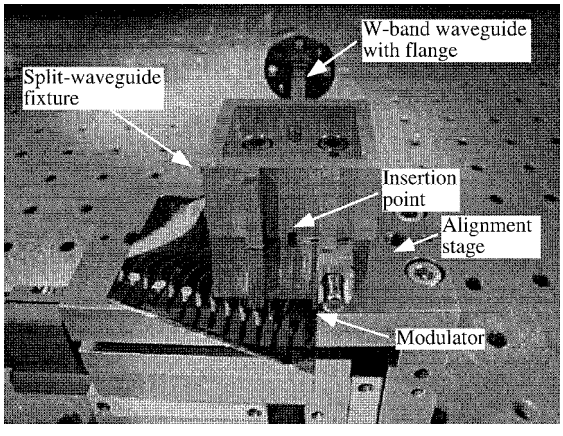

Fig. 9. Photograph of the 100 GHz modulator packaged with the W band waveguide. The optical fiber input and output are not shown.

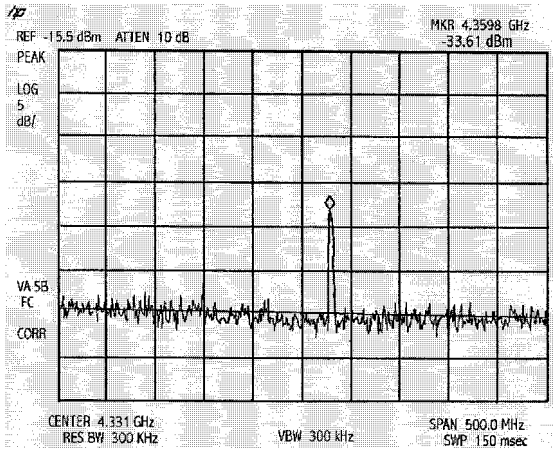

Fig. 10. The spectrum analyzer trace of the down converted signal at 95 GHz for the APII integrated phase modulator operating at 1310 nm.

The fabrication of polymer EO modulators on thin flexible substrates such as Mylar means that the modulator to some extent can be molded to fit a curvilinear surface. This opens some new possibilities for polymer modulators and polymer integrated optics in applications where the optical circuit might be molded to fit some specified contour such as that of a receiving antenna.

4. Polymer modulators with balanced outputs and the trimming of 3 dB output couplers

Mach-Zehnder modulators with 3 dB directional couplers on their output instead of a Y junction act as very fast optical switches. As shown in Fig. 11, the applied voltage toggles the light output between the two output waveguides. The balanced output modulator has applications both in digital communications and in analog communications. For example, if a sinusoidal modulation signal is applied to the modulator and it is properly biased, the light from the two outputs are both sinusoidally modulated but

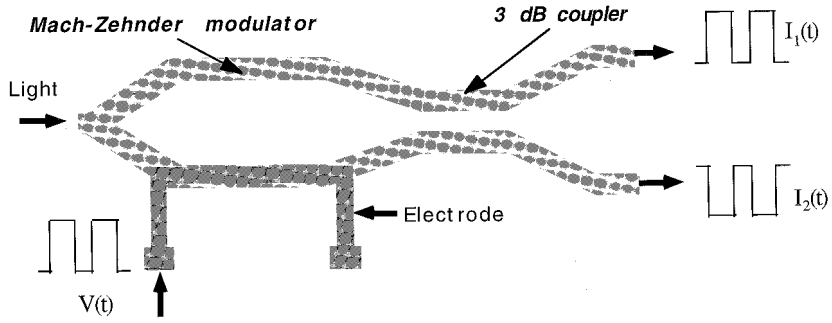

Fig. 11. Schematic of the optical modulator with balanced output. The applied voltage toggles the optical output between the upper and lower waveguides.

with the modulation 180° out of phase. If both of these signals are transmitted over a fiber optic system and detected at the far end by a balanced detector, the modulation signal can be extracted while the noise is canceled [22]. The applications of the balanced modulator require a very high extinction ratio between the two outputs. This means that when V_π is applied the light is essentially 100% switched from one output to the other. To achieve this, the output coupler must be very close to a 3 dB coupler, i.e. the input power from either one of its inputs is divided equally to the two output waveguides. The output coupler is based on directional coupling between two waveguides and they are highly sensitive to fabrication errors in the waveguide width, etch depth, and refractive indices. This is often hard to consistently achieve in the fabrication of the devices. To achieve good yield in the fabrication it is therefore important to have an in situ method to trim the coupler to exactly 3 dB at the desired wavelength. We have developed a trimming technique for polymer couplers which makes use of the unique photobleaching property of typical EO polymers [23].

The bleaching process used in the trimming is an irreversible photodecomposition of the chromophores [24]. The bleaching beam was the 488 nm output of the argon laser which is shorter than the wavelength of the principal absorption band of the EO chromophores used. We were able to confirm using Fourier transform infrared (FT-IR) and UV–Vis spectra of the photobleached films that photodecomposition occurred.

Waveguide couplers were designed to be nominally 3 dB and fabricated using our standard RIE ridge waveguide technology. The completed coupler is placed under a microscope and light is fiber coupled into one of the inputs as the power from each of the two outputs is monitored as shown in Fig. 12. The bleaching Ar^+ beam is delivered by a multimode fiber to one of the eyepiece bores of a binocular microscope to perform photobleaching. An eyepiece of the microscope was removed and the output end of the fiber is placed in the image plane of the objective lens. The microscope objective reduces the output pattern of the fiber and projects a beam spot onto the sample. The size of the fiber

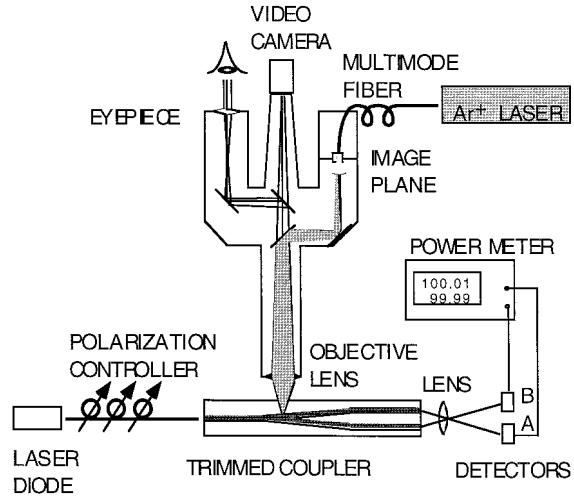

Fig. 12. Diagram for the use of a binocular microscope for the in situ trimming of polymer waveguide components. The argon laser bleaching beam is brought in through one eyepiece while the position of the bleaching beam is monitored through the other eyepiece or by a video camera.

core, the magnifying power of the microscope objective lens, and the axial position of the fiber tip determine the size of the spot. A spot size from 1 μm to >1 mm on the waveguide sample is obtainable. The position of the spot on the sample is observed through the other eyepiece or by a video camera on the microscope. Because the fiber tip is fixed to the microscope, its image always appears at the same place in the observation field of view when moving the microscope. This arrangement makes it very easy to position the beam spot to where the trimming should be performed.

To trim the directional coupler, the trimming beam spot is scanned for a fixed distance into the gap between the two coupling waveguides as the two outputs are monitored. The region scanned by the trimming beam has reduced refractive index which reduces the distance the tails of the waveguide modes extend into this coupling region. This in turn reduces the coupling coefficient and changes the output state of the two waveguides. Fig. 13 shows computer simulation studies of the output states of a typical polymer direction coupler as the bleached region is extended further into the coupling region. The ratio of the power in the two outputs can be trimmed to any desired number by changing the length of the bleached region.

To demonstrate the trimming, directional couplers were built with several different waveguide widths and coupling separations. The waveguide widths ranged from 2 to 10 μm and the separation ranged from 1 to 3 μm. The length of the coupling section varied from 300 to 2000 μm. The core layer, where the photobleaching occurs, was a thermal set polyurethane EO polymer that contains APII chromophores [20]. The absorption peak wavelength of this polymer is 560 nm. Fig. 14 shows the experimental results for the tuning of a directional coupler

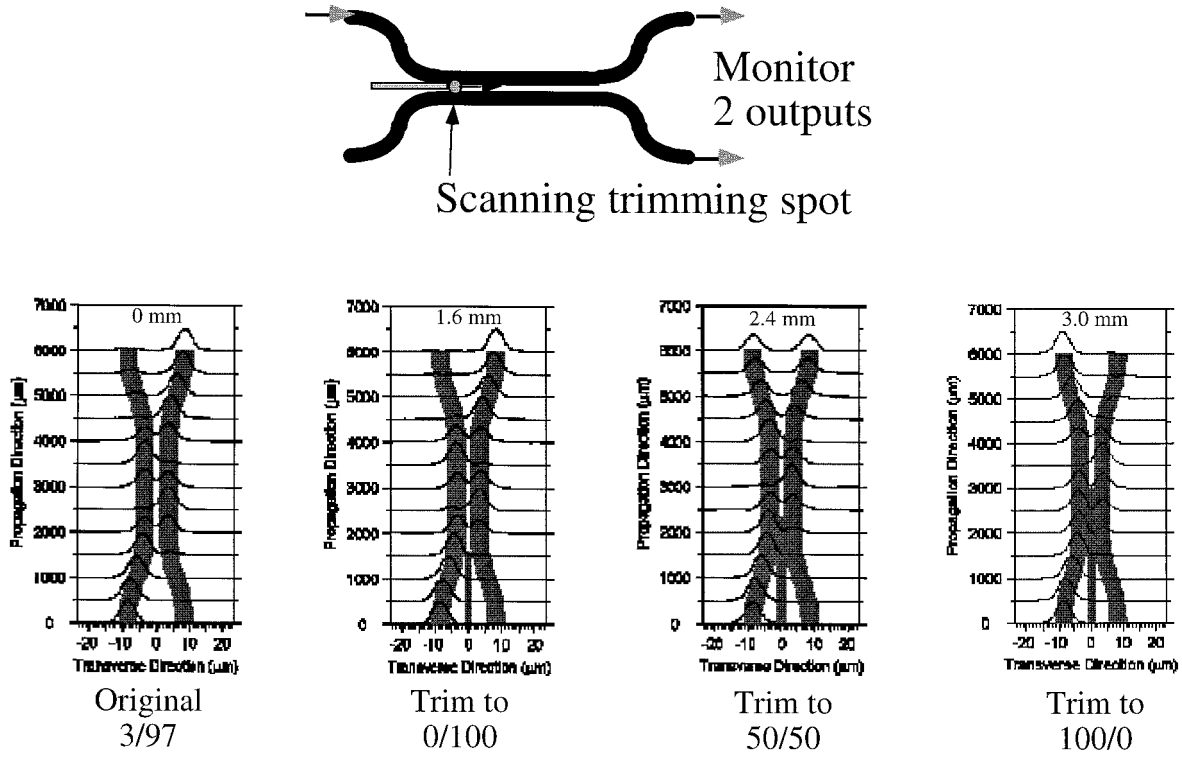

Fig. 13. Computer simulations of the trimming of a waveguide directional coupler by bleaching a portion of the coupling region. The four lower diagrams show the evolution of the optical input for various bleaching conditions. The distance the bleaching beam is advanced into the coupling region for each case can be seen.

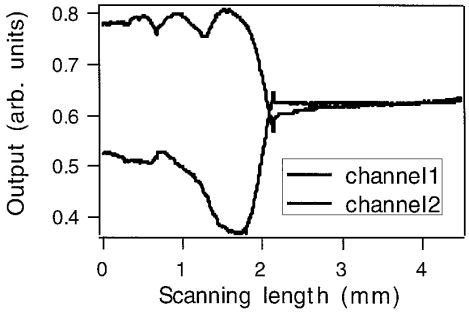

Fig. 14. Experimental measurement of the two outputs from a directional coupler as a function of the distance the bleaching beam is advanced into the coupling region. At ~2.1 mm the bleaching beam is turned off. There is typically a time transient before the amount of coupling reaches steady state. In this case it stabilizes to equal outputs on each output waveguide (3 dB coupler).

to achieve a 1:1 (3 dB) coupling ratio. The coupling ratio is monitored during the trimming, and the beam is turned off when the required 50/50 ratio is reached.

We fabricated a balanced output polymer modulator of the type shown in Fig. 11. The EO polymer used contained the FTC chromophore in a thermoset poly-urethane host [12]. The modulator had a V_π of 7 V @ 1300 nm. The modulator was demonstrated switching a 1 Gb/s digital data stream with complementary bit patterns on the two outputs.

5. Complex polymer EO guided wave devices – Photonic rf phase shifter

The fabrication of polymer integrated optics devices is a spin technology which can cover large areas and uses relative inexpensive substrates, typically silicon. This means that relatively large area and complex integrated optical circuits and devices can be built with relatively low cost using the polymer technology. The ability to combine both passive and active materials on the same substrate as discussed in the next section also makes large area complex polymer optical circuits appear promising. As an example of a complex active waveguide device using polymers we have recently demonstrated a wide-band millimeterwave photonic phase shifter.

Photonic millimeterwave phase shifters will play a key role in large phased array antennas [25]. Phased array antennas are composed of a large number of

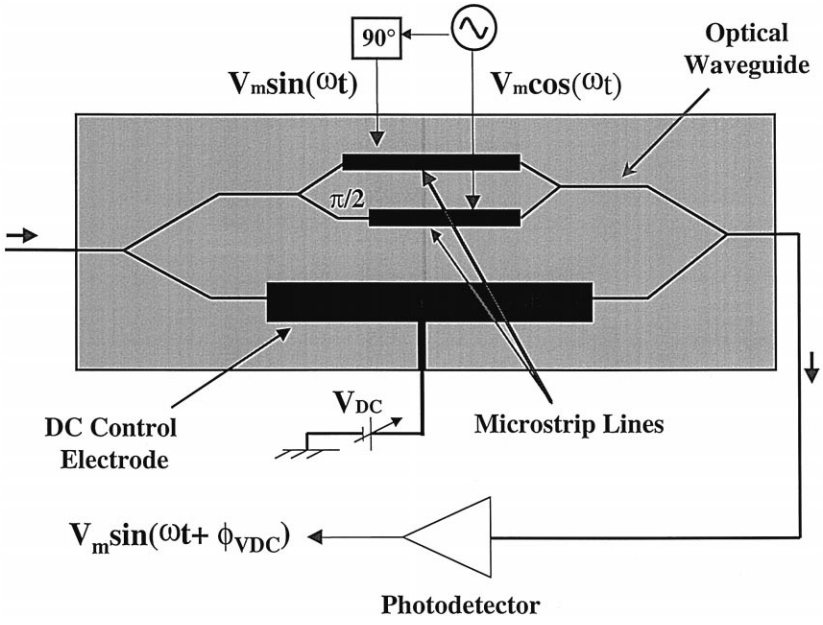

Fig. 15. Diagram of the photonic rf phase shifter. The function of this device is to modulate the signal at frequency ω onto the optical beam and to control the phase of this modulation by the dc voltage.

radiating elements with the phase and amplitude of the radiation from each element under independent control. By varying the phase and amplitude, the pattern of the array can be electronically scanned or its radiation patterned modified to avoid unwanted signals. The ideal phase shifter should be voltage-controlled, broadband, and lightweight. A very promising approach to delivering these controlled signals to each antenna is the use of low-loss optical fibers. The millimeterwave signal is modulated onto an infrared carrier and transmitted by fiber to the antenna where an optical detector recovers the millimeterwave signal, which is then radiated by the antenna. The fibers have the advantage of very low-loss, very low-weight, and possible use of low-noise optical amplifiers. The photonic phase shifter that we have demonstrated in the EO polymer combines into one unit the modulator and the millimeterwave phase shifter.

Fig. 15 is a schematic of the photonic phase shifter. It is composed of a Mach-Zehnder interferometer within a Mach-Zehnder interferometer. The millimeterwave signal is applied to each arm of the upper interferometer but with a 90° phase shift between the signals. If the amplitude of the drive signals is small, the frequency of the output of this interferometer is the infrared carrier frequency shifted by the rf frequency. A dc phase control voltage is applied to other arm of the complex interferometer. The phase of the rf modulation on the infrared carrier at the output is now controlled by the magnitude of the dc voltage. This device performs two functions; it modulates the rf on to the infrared beam and it controls the phase of that modulation.

We fabricated a polymer phase shifter using the same rib waveguide technology used to fabricate the Mach-Zehnder amplitude modulator discussed earlier. The EO polymer contained the CLD2 chromophore synthesized in Dalton's laboratory [26]. This high-$\mu\beta$ chromophore is similar to FTC except the thiophene moiety is replaced with a diene moiety. When covalently incorporated into a crosslinked polyurethane network the measured EO coefficient was 45 pm/V @ 1060 nm. The length of the electrodes was 16 mm and the V_π was 7 V. The total length of the device was 45 mm. Fig. 16 is a photograph of the phase shifter; four devices were fabricated on each silicon substrate.

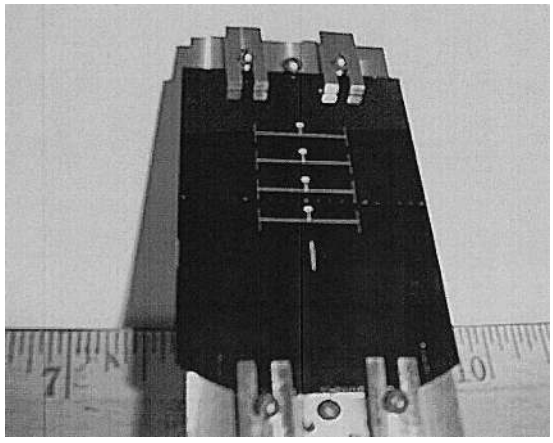

Fig. 16. Photograph of an array of four photonic rf phase shifters fabricated on a silicon substrate using the CLD2 chromophore in the thermal set polyurethane host.

The properties of the phase shifter were measured at a wavelength of 1310 nm and a rf frequency of 16 GHz. A low-frequency sawtooth waveform was applied to the control electrode and the rf phase measured by a network analyzer. Fig. 17 shows the results. In the ideal phase shifter the phase is linearly related to the control voltage. The data of Fig. 17 show that the phase is close to linear with some deviation at higher voltages. With an applied voltage of 7.8 V, the phase of the 16 GHz modulation could be shifted by 108°.

6. Integration of active and passive polymer devices using 3D integration

One of the advantages of the optical polymer technology is the ability to use different types of polymers within the same integrated optical circuit to perform specific functions. For example, EO polymers or light amplifying polymers could be integrated with low-loss passive polymers which provide the low-loss interconnections. Polymers which have been specifically designed for very low optical loss have been demonstrated in waveguides with losses as low as 0.1 dB/cm @ 1310 nm [27]. On the other hand, polymers specifically designed for high EO coefficients inevitably have higher loss. It is very difficult or impossible to achieve both very low loss and very high EO coefficients in the same material.

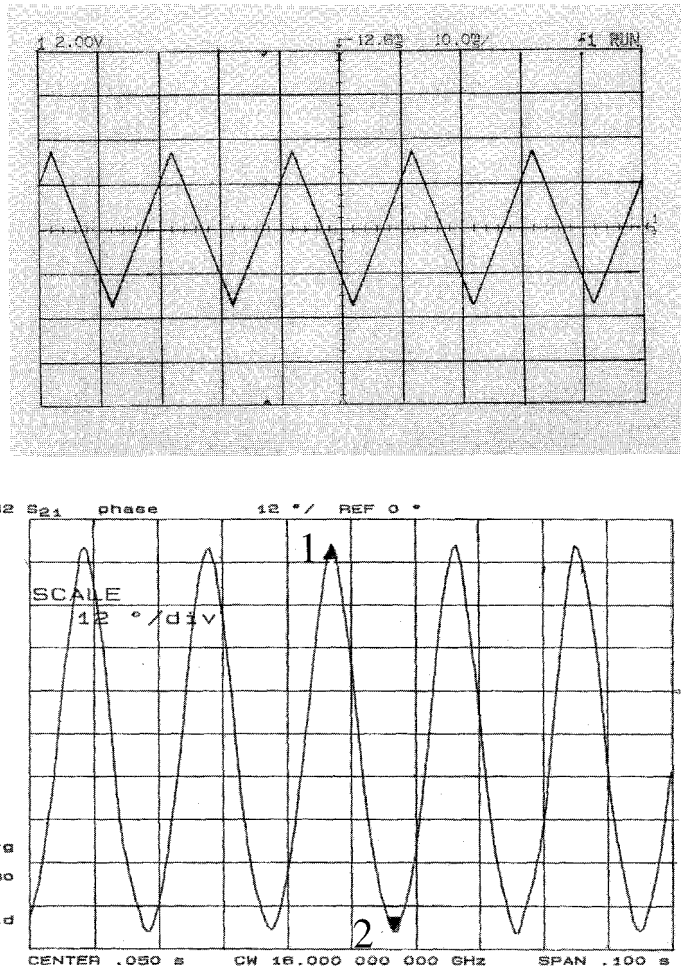

Fig. 17. Experimental measurements of the response of the photonic rf phase shifter at 16 GHz. Part (a) shows the low-frequency sawtooth voltage waveform applied to the phase control electrode. Part (b) shows the network analyzer measurement of the phase of the modulation. The rf phase shift between points 1 and 2 is 108° for a voltage change of 7.8 V. For the ideal phase shifter, the phase is linearly related to the voltage. Some distortion from linearity can be seen in part (b) at higher phase shifts.

In complex or large integrated optical circuits it would be advantageous to place the active polymer only in the portions of the circuit where it is required and thus minimize the transmission loss. While the adhesion and patterning problems in achieving the wedding of different polymers can sometimes be difficult, the greatest difficulty is often in achieving an optical mode match between the waveguides made from the different polymers [28]. The optimum optical mode pattern in the passive waveguides is typically nearly circular while that in a modulator is a relatively flat ellipse. This mismatch in shape and the difference in the index of refraction of the two polymers means the two waveguides cannot be simply butted together without suffering significant reflection and radiation loss at the junction. The use of the third vertical dimension provides a promising method to integrate different polymers while easily solving the mode match problem. In this approach, the interconnect waveguide pattern is first fabricated in a low-loss passive polymer system. The active polymer is then placed on top of this layer and patterned into the area where needed. Vertical coupling structures are then fabricated to channel the

light up into the active polymer and then back down again into the passive waveguides. We have developed fabrication techniques to provide 3D routing to transfer the beam between the passive and active polymer layers. To demonstrate the feasibility of the approach, we have integrated a poled polymer modulator with passive polymer waveguides.

The design of the polymer modulator integrated on top of a passive waveguide is shown in Fig. 18. The upper cladding, immediately below the upper electrode, and the lower cladding, below the lower electrode are not shown for clarity. The passive waveguide was designed to provide a close mode match to the standard 9 μm core fiber for fiber coupling. The critical fabrication technology is the etching of the vertical taper that was designed to adiabatically couple light to the higher index upper core layer which is made of a poled EO polymer. Vertical tapers can be reactive ion etched in O_2 and CF_4 either directly by shadow masks or through intermediate patterned photoresist layers. These techniques can create vertical slopes whose height can be accurately controlled from 1–15 μm and whose length can be set from 100–2000 μm [29].

Voltage applied to the electrodes will phase modulate the light or, if configured as a Mach-Zehnder interferometer, will amplitude modulate the light. In the modulator section, the passive core layer serves as the modulator lower cladding. After modulation, the power again transfers to the passive core for further routing. Both the adiabatic slopes and the lower electrode serve as inherent mode filters in the design to minimize stray light that exists in the device. While the mode in the passive waveguide was designed to be symmetric for good fiber coupling, the mode in the modulator was designed to be tightly confined to the active layer for good modulator efficiency. Ref. [6] reports the detailed design considerations and fabrication procedure.

Fig. 19 shows the final device dimensions and scaled cross-sections of the passive and active waveguide segments. The passive core and cladding layers consisted of NOA-73 and UV15LV, respectively. Thermoset polyurethane containing a DR 19 chromophore [13] composed the active upper core. The polyurethane layer was poled by an electric field to obtain the EO effect. The 6.5 cm long devices were fabricated on 3″ Si wafers as a substrate. The passive core waveguides in both sections were designed to be single mode at 1300 nm optical wavelength.

The integrated modulator was operated as a birefringence modulator. The modulation measured cor-

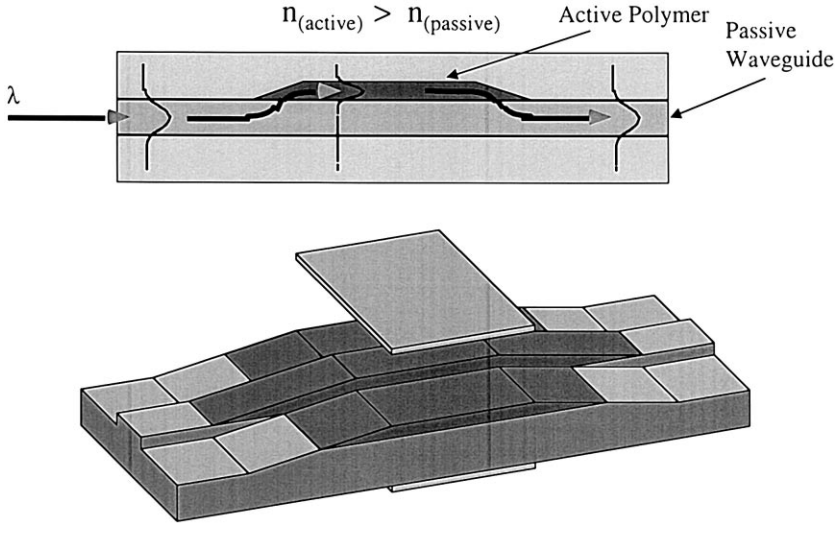

Fig. 18. The integration of active and passive polymers in an optical integrated circuit. The optical input to the passive waveguide is adiabatically transferred to the higher index active EO layer and then back down again. Because of the adiabatic nature of the transfer there is no mode mismatch. The lower picture shows the rib waveguides and the modulation electrodes. The upper cladding is not shown for clarity.

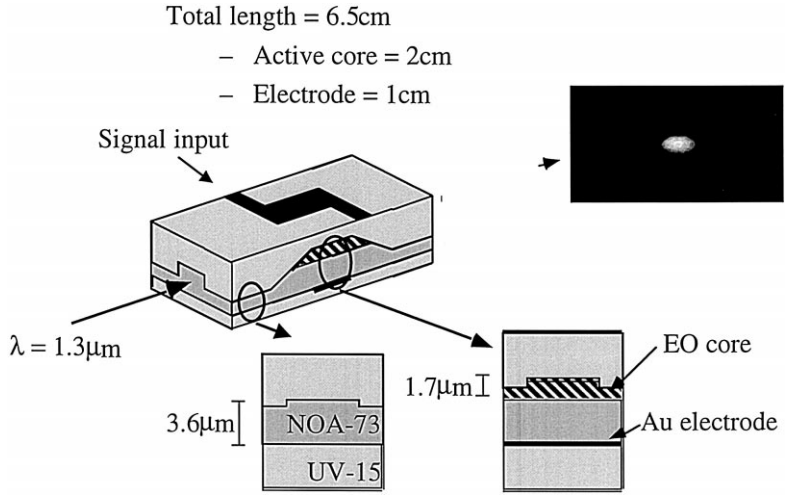

Fig. 19. Schematic of the integrated modulator showing dimensions and materials and a photograph of the single mode output at 1310 nm.

responded to an EO coefficient of $r_{33} = 12$ pm/V. Both the contrast observed in the modulation and the insertion loss of the device indicated that essentially all of the transmitted light coupled up into the modulator and back down again. Any light that remained in the lower waveguide is highly attenuated by the lower metal electrode. We also measured the insertion loss of several samples with different lengths of passive and active waveguide regions. From the known propagation losses in the two materials, we were again able to confirm that the light couples almost entirely up into the EO polymer and down again. Also from the known propagation losses in the passive and active materials, we were able to estimate the loss in the transition region to be ~ 1 dB. From beam propagation studies we expect the radiation losses in the tapers to be small and therefore believe the loss is due to scattering from the surface roughness of the etch. Better fabrication techniques should reduce this loss significantly.

7. Reducing the V_π of EO modulators by using a dc constant-bias voltage to achieve the full potential of high-$\mu\beta$ chromophores

The V_π of polymer Mach-Zehnder modulators can be reduced to the order of 1 V by using currently available materials and a dc constant-bias voltage on the modulator [30]. This approach achieves a very high degree of chomophore alignment due to the continued presence of the dc field and therefore makes full use of the potential of the high-$\mu\beta$ chromophores.

In almost all EO polymers, after the poling is completed and the poling field removed, there is a substantial partial relaxation of the chromophore alignment before it stabilizes at a residual value. This partial relaxation has been observed in both thermoplastic and thermosetting polymers and can significantly reduce the final value of r_{33}. In addition, Dalton et al. have shown that as the density of high-$\mu\beta$ chromophores is increased there is a tendency for the chromophores to aggregate and not contribute to the EO effect unless special molecular designs are used [3]. The combination of the chromophore aggregation and the orientational relaxation, both of which are increased with the high-$\mu\beta$ chromophores, is believed to be the reason that the new chromophores have not produced the high EO coefficients that the electric-field-induced second-harmonic (EFISH) measurements on the chromophores would predict. The dc constant-bias voltage partially overcomes the relaxation and the aggregation.

To demonstrate the low-V_p operation, optical channel waveguide modulators were built as shown

in Fig. 20. A number of EO polymers were used including two high-$\mu\beta$ materials:

(a) an isophorone based chromophore, APII ($\mu\beta \approx 3\,160 \times 10^{-48}$ esu), doped in PMMA host at 45 wt% [20];

(b) a high-$\mu\beta$ chromophore, FTC ($\mu\beta \approx 15\,000 \times 10^{-48}$ esu), based on a tricyanobutadiene acceptor incorporating a furan-derivative ring, doped in PMMA at 22 wt% [12].

We also used a DR1-PMMA side-chain thermoplastic EO polymer [31] to study the effectiveness of the biased operation scheme on small-$\mu\beta$ materials. In this material, one end of the DR1 chromophore is covalently attached to the PMMA chain. This polymer was purchased from IBM Almaden Research Center as a commercial product.

A variety of cladding materials were used. Epoxylite 9653 and Norland UV curable adhesives were used for the lower cladding. Depending on the compatibility between UV curable adhesives and the EO polymers, either UV curable epoxies (Norland 61 and 73) or water-soluble polymers (PVA and PAA) were used for the upper cladding. The polymer layers were spin-coated and the trenches for the inverted rib waveguides were made by photolithography and low-loss oxygen reactive ion etching. No attempt was made to increase the conductivity of the cladding layers to improve the poling efficiency. The modulators were 2.5 cm long and the lengths of the top electrodes were 2–2.4 cm. The endfaces were prepared by cleaving and dicing. The temperature of the modulator was maintained by a closed-loop system consisting of a temperature controller, a thermoelectric cooler (TEC), and a thermistor. The lower electrode was grounded, and a dc bias voltage was applied to the top electrode to create a constant electric field that actively aligns the chromophores. The AC modulating voltage was coupled to the top electrode through a bias tee circuit consisting of a capacitor and a resistor. Light of 1310 nm wavelength was coupled into the optical waveguide from the single mode fiber pigtail of a 1.3 mW semiconductor laser. The device was operated as a birefringent modulator by simultaneously launching both TE and TM modes into the waveguide with light polarized at 45°.

The measured V_p of a modulator made of APII/PMMA as a function of the dc bias voltage at room temperature and as a function of temperature for a constant 300 V bias is shown in Fig. 21. V_π decreases as both the bias voltage and the sample temperature increases as expected since both effects more efficiently align the chromophores. The alignment took 2–5 min to reach the stable level. At 40–45°C and with a bias voltage of 300 V (60 V/μm), these birefringent modulators exhibited V_p's in the range of 1.57 ± 0.03 to 1.83 ± 0.03 V. The V_p can be reduced by 2/3 if the sample is operated as a TM Mach-Zehnder modulator. No increase of V_p was observed when these samples were cooled to

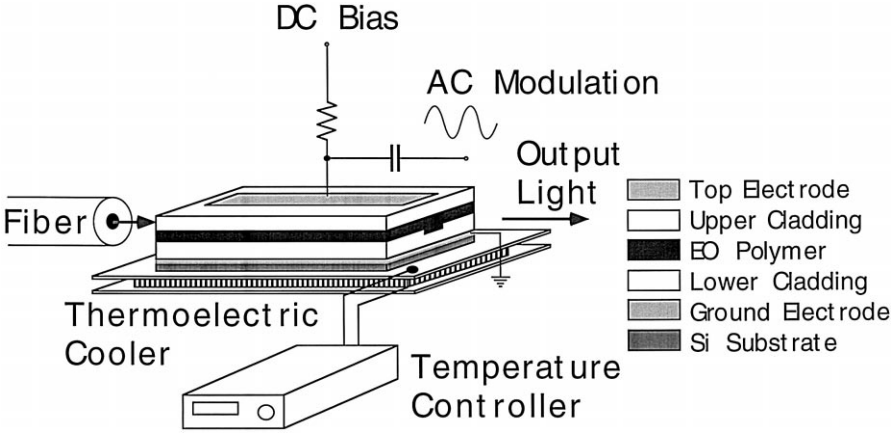

Fig. 20. Diagram of the constant-bias low-voltage polymer modulator. The constant-bias voltage keeps a high degree of chromophore alignment and a high EO coefficient.

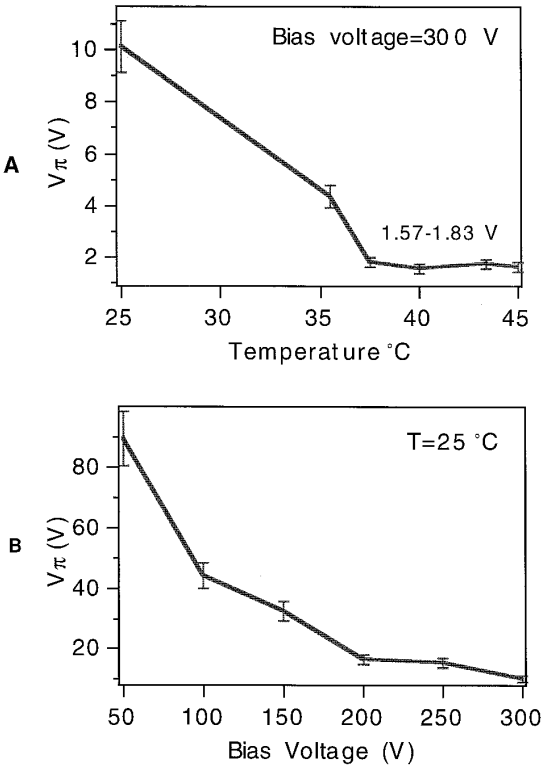

Fig. 21. Experimental measurements of the V_π of the constant-bias modulator. Part A shows V_π as a function of the substrate temperature at 60 V/μm bias electric field. V_π is under 2 V at 40°C and above. The EO material contained the APII chromophore and this V_π corresponds to $r_{33} = 70$ pm/V. After alignment, V_π remains steady if the modulator is returned to room temperature but the bias voltage remains. Part B shows the poling of the material if the temperature is constant and the bias voltage increased.

room temperature with the bias voltage applied. If one assumes that $r_{33} = 3r_{13}$, the measured V_p corresponds to $r_{33} = 70$ pm/V. The modulators made of FTC/PMMA also give V_p of 1.5–1.8 V with a bias voltage of 1000 V (167 V/μm) at 70°C which corresponds to $r_{33} = 83$ pm/V. The IBM DR1 material gave an $r_{33} = 22$ pm/V which is high for this material.

Chen et al. [32] have discussed the temporal stability of these devices and the prospects for packaging the modulators with a dc constant-bias voltage. Outside of the device applications, this work clearly shows the high potential of the available EO chromophores and the large EO coefficients that are possible in highly aligned systems.

8. Maskless fabrication of EO polymer devices by simultaneous direct laser writing and electric poling of channel waveguides

EO polymers are unique in that short-wavelength visible or UV radiation can alter the alignment of the chromophores in the material to change both the index of refraction and the degree of alignment during poling. Based on these effects, one can simultaneously directly laser write and electric field pole a pattern of arbitrary channel waveguides that have the EO effect in selected regions [33]. As shown in Fig. 22, the sample to be written with channel waveguides consists a substrate, gold ground electrode, three spun layers of polymer (upper and lower passive cladding and active core), and a semi transparent upper electrode. For fiber coupling, the endfaces of the sample are either cleaved or cut with a dicing saw before waveguide writing. In this case, the core layer used is a disperse red 19 (DR19) containing thermoset polymer [13]. The absorption peak of the DR19 chromophores is at 470 nm. Waveguide writing is done with a focused beam of 488 or 515 nm from a cw Ar^+ laser. When the beam scans across the sample without applying the poling voltage or in the area outside the top electrode, the chromophores in the path of the beam are preferentially aligned perpendicular to the substrate with, on average, equal number of chromophore dipoles pointing up and down due to photo-orientation [34,35]. The partial alignment increases the refractive index for TM polarization and a passive channel waveguide that only supports the TM mode is made. When the laser beam scans across the area with a top electrode and a poling voltage is applied, the chromophores are preferentially aligned in the direction of the poling field due to a process known as light-assisted electric poling [36]. An EO channel waveguide is formed.

The waveguides are written using a binocular microscope with the writing beam fed through one eyepiece and focused on the sample similar to that shown in Fig. 12. For this work, the spot size of the beam on the sample is adjustable from 1 to 50 μm

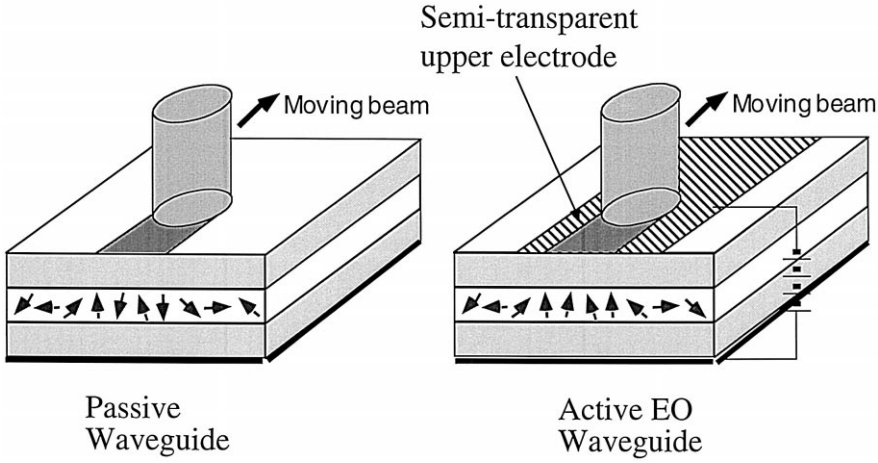

Fig. 22. Schematic of the maskless writing of electro-optic polymer devices by simultaneous direct laser writing and electric field poling of channel waveguides. In the first diagram, no poling voltage is present and the laser beams increases the index of refraction for the TM polarization by photo orientation but does not align the material for the EO effect. In the second diagram, the poling field is present and the laser beam both increases the index of refraction for the TM polarization and aligns the chromophores to achieve the EO effect through light-assisted electric field poling.

and the typical unpolarized writing beam power was 1 mW; a poling field of 100 V/μm is used. During writing, the substrate temperature is elevated to assist in the dipole orientation. Fig. 23 shows how this technique is used to fabricate EO modulators. The active waveguides are written with the poling voltage on and must be under the electrode. The passive waveguides are written with the poling voltage off or in the region outside the electrode. Amplitude modulators were demonstrated with V_π as low as 8 V in a 25 mm long device at a wavelength 1300 nm. This corresponds to an r_{33} of ~ 17 pm/V which is significantly higher than the 5 pm/V that can be achieved in this material @100 V/μm.

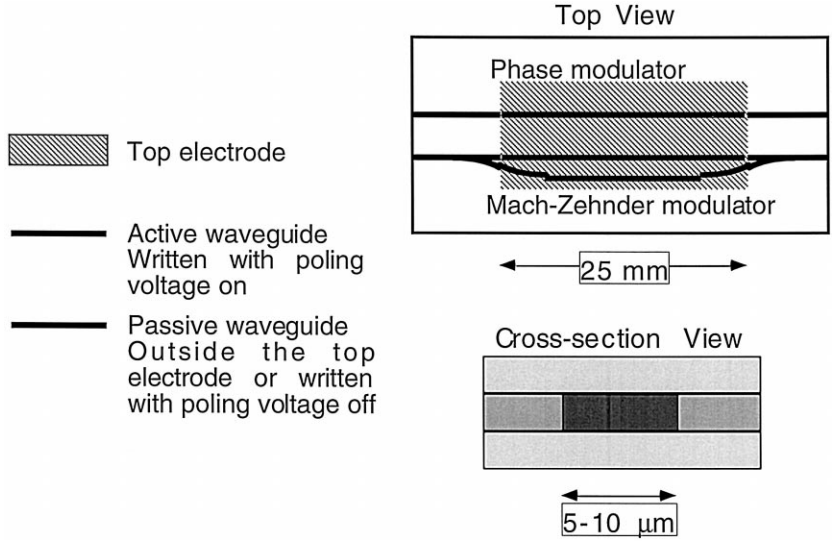

Fig. 23. Diagram of the direct laser writing of EO polymer modulators. The scanned laser beam without the need for photolithography masks directly writes both a phase modulator and a Mach-Zehnder amplitude modulator.

This technique is a fast and effective method to prototype new EO devices, it requires no lithography mask, and one can achieve higher EO coefficients than with conventional electrode poling.

Acknowledgements

The authors would like to acknowledge the vital support of AFOSR, BMDO, ONR, DARPA, and TRW.

References

[1] D.M. Burland, R.D. Miller, C.A. Walsh, Chem. Rev. 94 (1994) 31–77.
[2] G.A. Lindsay, Polymers for second-order nonlinear optics, in: G.A. Lindsay, K.D. Singer (Eds.), American Chemical Society Symposium Series, 601, Am. Chem. Soc., Washington, DC, 1995, p.11.
[3] L.R. Dalton, A.W. Harper, B.H. Robinson, Proc. Natl. Acad. Sci. USA 94 (1997) 4842.
[4] D. Chen, H.R. Fetterman, A. Chen, W.H. Steier, L.R. Dalton, W. Wang, Y. Shi, Appl. Phys. Lett. 70 (1997) 3335–3337.
[5] S. Kalluri, M. Ziari, A. Chen, V. Chuyanov, W.H. Steier, D. Chen, B. Jalali, H. Fetterman, L.R. Dalton, Phot. Tech. Lett. 8 (1996) .
[6] S.M. Garner, S.S. Lee, V. Chuyanov, A. Yacoubian, A. Chen, W.H. Steier, J. Zhu, J. Chen, L.R. Dalton, ICAPT '98, Ottawa, ON.
[7] Uniphase Telecommunications Products, Bloomfield, CT 06002
[8] Lucent Technologies, Breinigsville, PA 18031.
[9] K. Noguchi, O. Mitomi, H. Miyazawa, J. Lightwave Tech. 16 (1998) 615–619.
[10] M. Ziari, A. Chen, S. Kalluri, W.H. Steier, Y. Shi, W. Wang, D. Chen, H.R. Fetterman, Nonlinear Optical Polymer: From Molecules to χ^2 Applications, in: G. Lindsey, K. Singer (Eds.), Am., Chem. Soc., Washington, DC, 1994.
[11] A. Chen, F.I. Marti-Carrera, S. Garner, V. Chuyanov, W.H. Steier, Org. Thin Films for Photonics Applications, Opt. Soc. Am. Tech. Digest Ser. 14 (1997) 152–154.
[12] F. Wang, A.S. Ren, M. He, M. Lee, A.W. Harper, L.R. Dalton, H. Zhang, S.M. Garner, A. Chen, W.H. Steier, Am. Chem. Soc. Meet., Boston, MA, 1998, Polymer Prepr. 1065-7.
[13] Y. Shi, W.H. Steier, M. Chen, L. Yu, L.R. Dalton, Appl. Phys. Lett. 60 (1992) 2577–2579.
[14] Epoxylite, Irvin, CA 92713-9671.
[15] Norland Products, Brunswick, NJ 08902.
[16] C.C. Teng, M.A. Mortazavi, G.K. Boudoughian, Appl. Phys. Lett. 66 (1995) 667–669.
[17] A. Chen, V. Chuyanov, F.I. Marti-Carrera, S. Garner, W.H. Steier, J. Wang, S. Sun, L.R. Dalton, SPIE (Soc. Photo-Opt. Instrum. Eng.) Photonics West, Feb. 1997, Pap. 3005-11.
[18] W.B. Jackson, N.M. Amer, A.C. Boccara, D. Fournier, Appl. Opt. 20 (1981) 1333–1344.
[19] D. Chen, H.R. Fetterman, B. Tsap, A. Chen, W.H. Steier, L.R. Dalton, Topical Meeting on Organic Thin Films for Photonic Applications, Long Beach, CA, Oct. 1997 (also submitted to Appl. Phys. Lett.).
[20] J. Chen, J. Zhu, A.W. Harper, F. Wang, M. He, S.S.H. Mao, L.R. Dalton, A. Chen, W.H. Steier, Polymer Prepr. 38 (1998) 215–216.
[21] W. Wang, D. Chen, H.R. Fetterman, Y. Shi, W.H. Steier, L.R. Dalton, Appl. Phys. Lett. 67 (1995) 1806–1808.
[22] G.L. Abbas, V.W.S. Chan, T.K. Yee, IEEE J. Lightwave Tech. LT3 (1985) 1110–1122.
[23] A. Chen, V. Chuyanov, F.I. Marti-Carrera, S. Garner, W.H. Steier, S.S.H. Mao, Y. Ra, L.R. Dalton, Photonic Technol. Lett. 9 (1997) 1499–1501.
[24] D.G. Girton, S.O.L. Kwiatkowski, G.F. Lipscomb, R.S. Lytel, Appl. Phys. Lett. 58 (1991) 1730.
[25] J.F. Coward, T.K. Yee, C.H. Chalfant, P.H. Chang, IEEE J. Lightwave Tech. 11 (1993) 2201–2205.
[26] C. Zhang, A.S. Ren, F. Wang, L.R. Dalton, S.-S. Lee, W.H. Steier, Am. Chem. Soc. Meet., Anaheim, CA, Spring 1997.
[27] R. Yoshimura, M. Hikita, S. Tomaru, S. Imamura, J. Lightwave Tech. 16 (1998) 1030–1038.
[28] T. Watanabe, M. Hikita, M. Amano, Y. Shuto, S. Tomaru, J. Appl. Phys. 83 (1998) 639–649.
[29] S. Garner, V. Chuyanov, A. Chen, A. Yacobian, W.H. Steier, L.R. Dalton, LEOS '97, San Francisco, CA, 1997.
[30] A. Chen, V. Chuyanov, H. Zhang, S. Garner, W.H. Steier, J. Chen, J. Zhu, M. He, S.S.H. Mao, A. Harper, L.R. Dalton, Opt. Lett. 23 (1998) 478–480.
[31] S. Matsumoto, K. Kubodera, T. Kurihara, T. Kaino, Appl. Phys. Lett. 51 (1987) 1–2.
[32] A. Chen, V. Chuyanov, H. Zhang, S. Garner, S.-S. Lee, W.H. Steier, J. Chen, F. Wang, J. Zhu, M. He, Y. Rao, S.S.H. Mao, A.W. Harper, L.R. Dalton, H.R. Fetterman, Proc. SPIE (Soc. Photo-Opt. Instrum. Eng.) 3281 (1998) also submitted to Opt. Eng.
[33] A. Chen, V. Chuyanov, S. Garner, W.H. Steier, J. Chen, Y. Ra, S. Mao, G. Lin, L.R. Dalton, LEOS '97, San Francisco, CA, 1997.
[34] Y. Shi, W.H. Steier, L. Yu, M. Chen, L.R. Dalton, Appl. Phys. Lett. 59 (1991) 2935–2937.
[35] Z. Sekkat, J. Wood, E.F. Aust, W. Knoll, W. Volksen, R.D. Miller, J. Opt. Soc. Am. B 13 (1996) 1713–1724.
[36] X.L. Jiang, L. Li, J. Kumar, S.K. Tripathy, Appl. Phys. Lett. 69 (1996) 3629–3631.